TUM SCHOOL OF COMPUTATION,
INFORMATION AND TECHNOLOGY (CIT)

TECHNICAL UNIVERSITY OF MUNICH

Report Submitted to Praktikum Robot Modelling and Identification
(IN2106)

Experiment 2: Independent Joint Control

Jesus Arturo Sol Navarro, Sarah Weber

TECHNICAL UNIVERSITY OF MUNICH

Report Submitted to Praktikum Robot Modelling and Identification (IN2106)

Experiment 2: Independent Joint Control

Author:	Jesus Arturo Sol Navarro, Sarah Weber
Lecturers:	Prof. Dr. M.Sc. Alexander König, M.Sc. Moritz Eckhoff, Moein Forouhar
Submission Date:	May 15, 2025

We confirm that this report is my our own work and we have documented all sources and material used.

Munich, May 15, 2025
Jesus Arturo Sol Navarro, Sarah Weber

Contents

1 IJC - Independent Joint Control

1.1 Task 1

Model the motor in the block diagram in Fig. 1.1 using Simulink gain and Integrator, Second Order block. The model has two inputs, namely disturbance d and armature voltage V_a, and two outputs, namely motor position θ and velocity $\dot{\theta}$. The motor parameters are listed in Table 1.1.

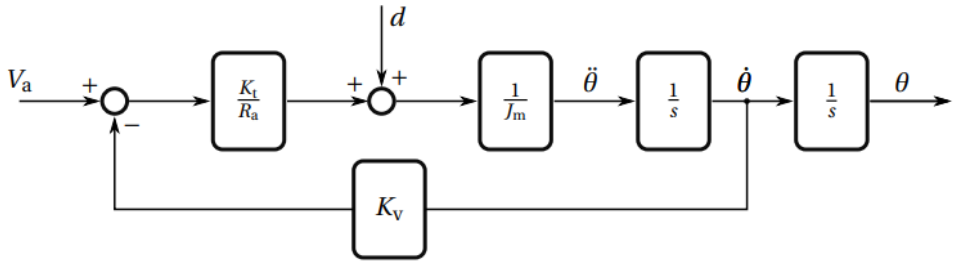

Figure 1.1: Block diagram of DC motor

Table 1.1: DC motor parameters

Variable name	Physical meaning	Value	Unit
θ	Rotor position	System output	rad
V_c	Control voltage	Control variable	V
V_a	Armature voltage	System input	V
G_v	Amplifier gain		
R_a	Armature resistance	0.3	Ω
K_v	Motor constant	0.5	Vs/rad
K_t	Torque constant	0.5	Nm/A
J_m	Motor moment of inertia	6	Kg m^2

Figure 1.2 illustrates the time response of the motor's angular velocity $\dot{\theta}$ when a constant armature voltage input of $V_a = 1$ V is applied, with no external disturbance ($d = 0$). As shown in the graph, the motor accelerates initially and gradually approaches a steady-state velocity of 2 rad/s.

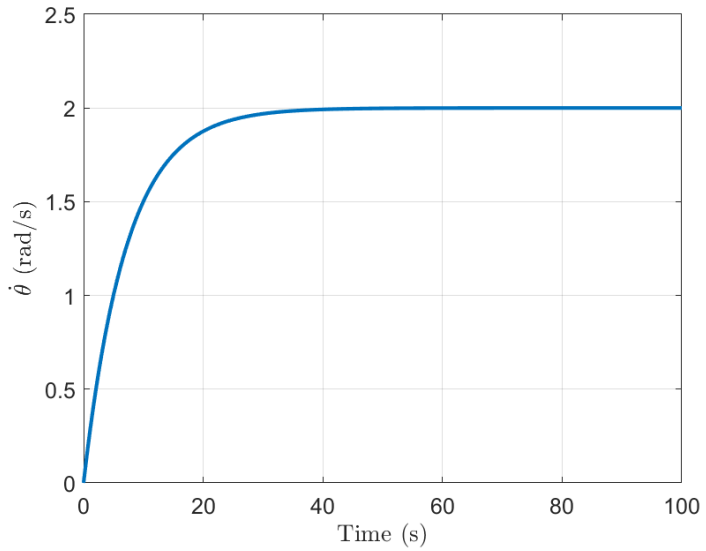

Figure 1.2: Motor angular velocity response to a constant voltage input ($V_a = 1$ V, $d = 0$).

1.2 Task 2

Add the amplifier (which is the gain G_v) and create the control voltage signal V_c.

Figure 1.3 shows the closed-loop time response of the motor position θ tracking the desired set-point $\theta_d = 1$ rad. The system is configured with position feedback and an amplifier gain of $G_v = 1$, while no external disturbance is applied. As observed in the plot, the motor position converges to the desired set-point.

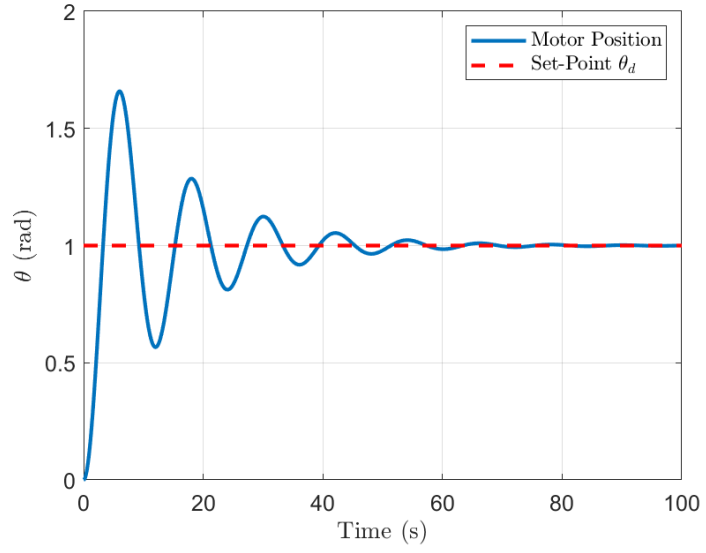

Figure 1.3: Motor position response ($\theta_d = 1$ rad, $G_v = 1$, $d = 0$).

Figure 1.4 shows the closed-loop motor position response θ when subjected to a constant external disturbance of 1 Nm, while tracking a set-point of $\theta_d = 1$ rad. The disturbance introduces a noticeable deviation from the desired trajectory, causing a steady-state error in the motor

position. Unlike the disturbance-free case, the system does not stabilizes to the set-point. This demonstrates the system's limited disturbance rejection capability and suggests the need for a more robust controller.

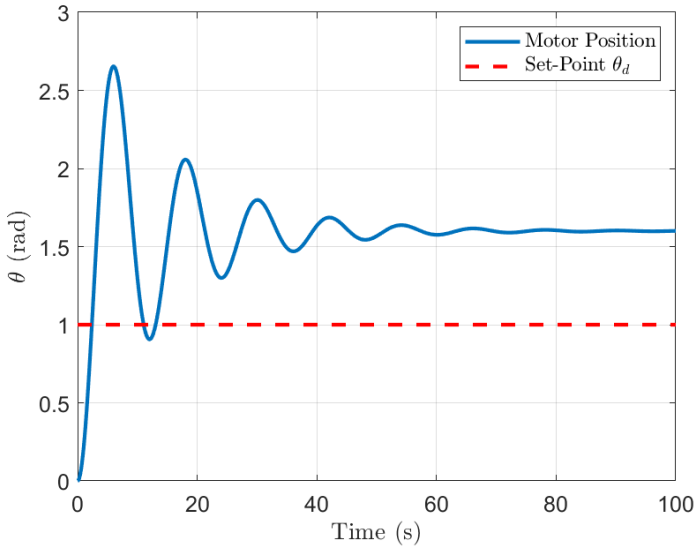

Figure 1.4: Motor position response ($\theta_d = 1$ rad, $G_v = 1$, $d = 1$ Nm).

The closed-loop transfer functions describe how the system output $\Theta(s)$ responds to both the reference input $\Theta_r(s)$ and external disturbances $D(s)$. Eq. 1.1 characterizes the response to the reference input, while Eq. 1.2 models the system's sensitivity to disturbances .

$$\frac{\Theta(s)}{\Theta_r(s)} = \frac{1}{\frac{J_m R_a}{K_t G_v} s^2 + \frac{K_v}{G_v} s + 1} = \frac{1}{\frac{3.6}{G_v} s^2 + \frac{1}{2G_v} s + 1} \tag{1.1}$$

$$\frac{\theta(s)}{d(s)} = \frac{1}{J_m s^2 + K_v s + \frac{K_t G_V}{R_a}} = \frac{1}{6s^2 + \frac{1}{2} s + \frac{5G_V}{3}} \tag{1.2}$$

The effect of G_V on system behavior can be directly interpreted from the closed-loop transfer functions. In the transfer function 1.1, increasing G_V results in a decrease in the coefficients of both the s^2 and s terms. This causes the closed-loop poles to move closer to the imaginary axis in the complex plane, leading to a less damped, more oscillatory system response.

In contrast, in the transfer function 1.2, G_V appears only in the constant term. Increasing G_V shifts the poles further to the left on the real axis, thereby increasing system stability and improving its ability to reject disturbances. This means that a higher G_V reduces the steady-state effect of disturbances on the output.

Validated in Fig. 1.5, a higher G_v can improve tracking $\theta \to \theta_d$, but leads to higher oscillation frequencies. Therefore, the impact of the disturbance can be reduced by increasing G_v and the gain must be carefully selected to achieve a suitable balance between disturbance rejection, tracking performance, and stability.

In Fig. 1.6, the root locus analysis of the transfer function (Eq. 1.1) is presented. Four distinct pole locations corresponding to different values of G_V were marked along the locus to facilitate

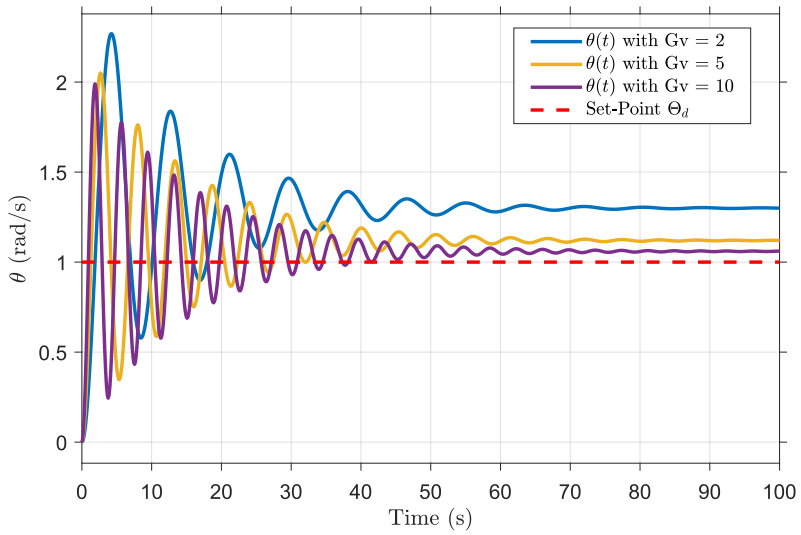

Figure 1.5: Comparison of the motor position response $\theta(t)$ under a 1 Nm disturbance with different values for the gain G_v. The plot shows the effect of increasing the gain G_v.

comparison with the different system responses illustrated in Fig. 1.5. Both figures support the observation that higher oscillation frequencies arise in systems with larger values of G_V, as the imaginary part of the poles directly determines the frequency of oscillation. This highlights a fundamental trade-off: while increasing G_V enhances system performance in terms of reference tracking and disturbance rejection, it may also reduce damping and lead to excessive oscillations.

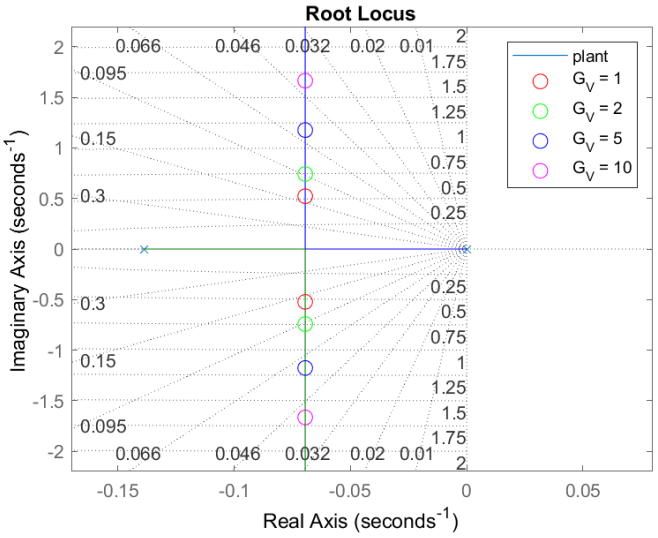

Figure 1.6: Root locus plot of the closed-loop system with the forward gain G_V as the variable parameter.

1.3 Task 3

The following transfer function represents the closed-loop system with a PI controller applied to the plant.

$$\frac{\Theta(s)}{\Theta_r(s)} = \frac{K_m\left(K_P s + K_I\right)}{s^2(1+sT_m) + K_m\left(K_P s + K_I\right)} = \frac{2\left(K_P s + K_I\right)}{s^2(1+7.2s) + 2\left(K_P s + K_I\right)} \tag{1.3}$$

Since MATLAB's `rlocus` function places the variable gain K in the feedback path, we rewrite the original system as an open-loop transfer function where the controller is in the forward path and gain K is swept for root locus analysis.

$$\frac{\Theta(s)}{\Theta_r(s)} = \frac{L(s)}{1+KL(s)}, \quad \text{where } L(s) = \frac{K_m(K_P s + K_I)}{s^2(1+sT_m)} = \frac{2K_P(s+\frac{K_I}{K_P})}{s^2(1+7.2s)} \tag{1.4}$$

In order to analyze the steady-state error, we apply the Final Value Theorem to the error function, which yields

$$e_{ss} = \lim_{t\to\infty} e(t) = \lim_{s\to 0} s\cdot E(s) = \lim_{s\to 0}\left[1 - \frac{L(s)}{1+KL(s)}\right] = \lim_{s\to 0}\left[1 - \frac{1}{\frac{1}{L(s)}+K}\right] = 1 - \frac{1}{K} \tag{1.5}$$

with

$$\lim_{s\to 0} L(s) \to \infty. \tag{1.6}$$

Thus, for $e_{ss} = 0$ we conclude that $1 - \frac{1}{K} = 0$. Therefore, we keep $K = 1$ for this task. If the gain K is introduced in the forward path (as it is intended for the root locus method), then any value of $K > 0$ can be chosen as the steady-state error yields

$$e_{ss} = \lim_{s\to 0}\left[1 - \frac{KL(s)}{1+KL(s)}\right] = \lim_{s\to 0}\left[1 - \frac{K}{\frac{1}{L(s)}+K}\right] = 1 - \frac{K}{K} = 0. \tag{1.7}$$

Another way to compensate for the scaling of the output, if the gain K is only the feedback path, is to place a gain K before the feedback.
The equation (1.3) shows that the PI-controller adds a pole at $p_{PI} = 0$ and a zero at $z_{PI} = K_i/K_p$ to the system. Furthermore, the open-loop transfer function of the motor shows that we have two poles at $p_1 = 0$ and $p_2 = -\frac{1}{7.2} = -0.139$. Thus, modifying the ratio K_i/K_p alters the root locus shape. This provides a mechanism to influence pole locations and ensure closed-loop stability. If the zero z_{PI} is between p_{PI}/p_1 and p_2, then it will attract the poles from 0 into the left half complex plane $\mathbb{C}^-$. Otherwise, the pole p_2 will reject the other poles into $\mathbb{C}^+$. This behavior can be observed by comparing Fig. 1.7 and Fig. 1.8. Thus, choosing values for $K_i/K_p < 0.139$ will ensure a stable system.
To simulate the closed-loop system, we designed our Simulink model as depicted in Fig. 1.9. In Fig. 1.10, the results for a simulation with disturbance set to $d = 1$ Nm and without disturbances are shown.

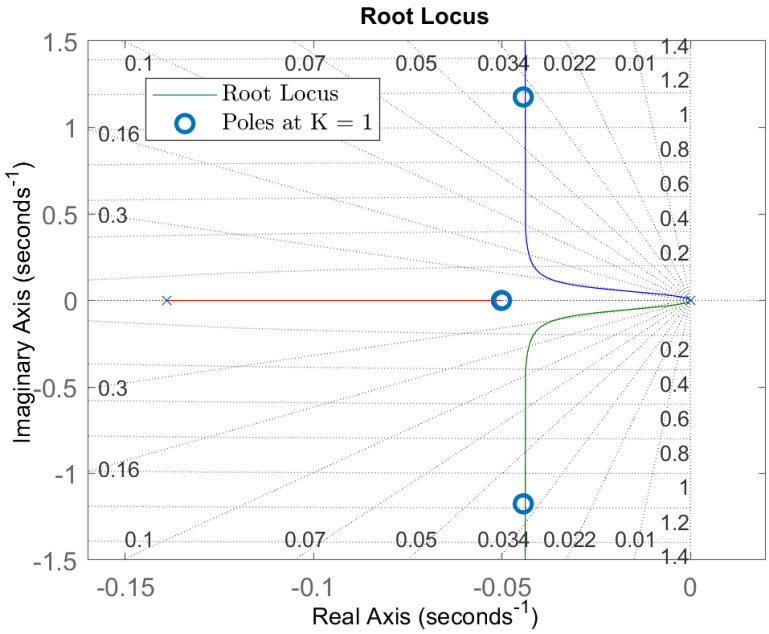

Figure 1.7: Root locus plot for the ratio $K_i/K_p = 0.25/5 = 0.05 < 0.139$. All poles are in $\mathbb{C}^-$, and thus, the system is stable.

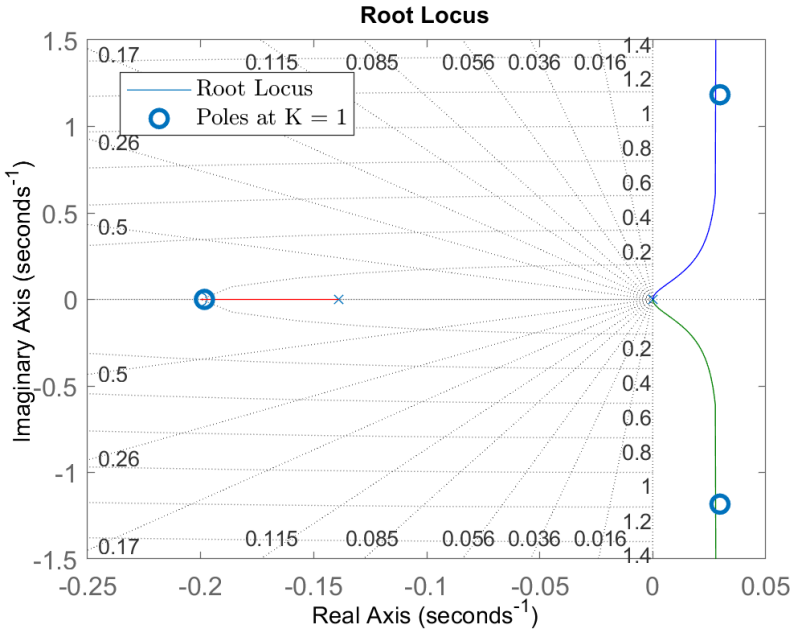

Figure 1.8: Root locus plot for the ratio $K_i/K_p = 1/5 = 0.25 > 0.139$. Two poles are always in $\mathbb{C}^+$, and thus, the system is not stable for any K.

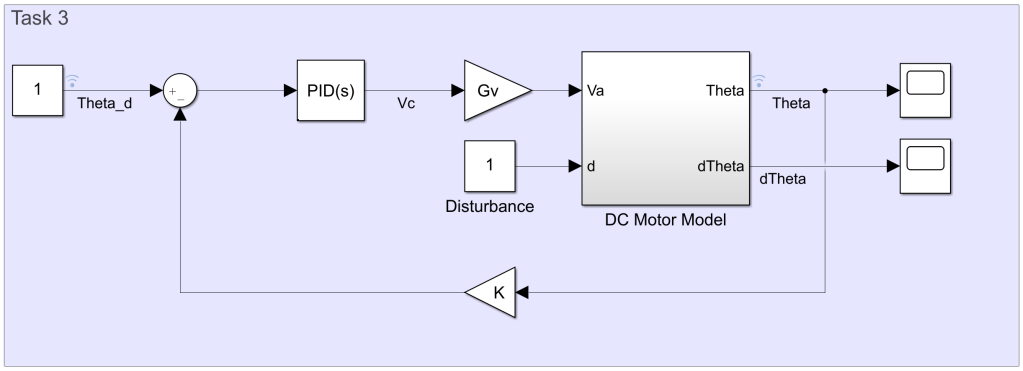

Figure 1.9: Simulink model with gain K in the feedback path and a PI-controller in the forward path ($K_D = 0$).

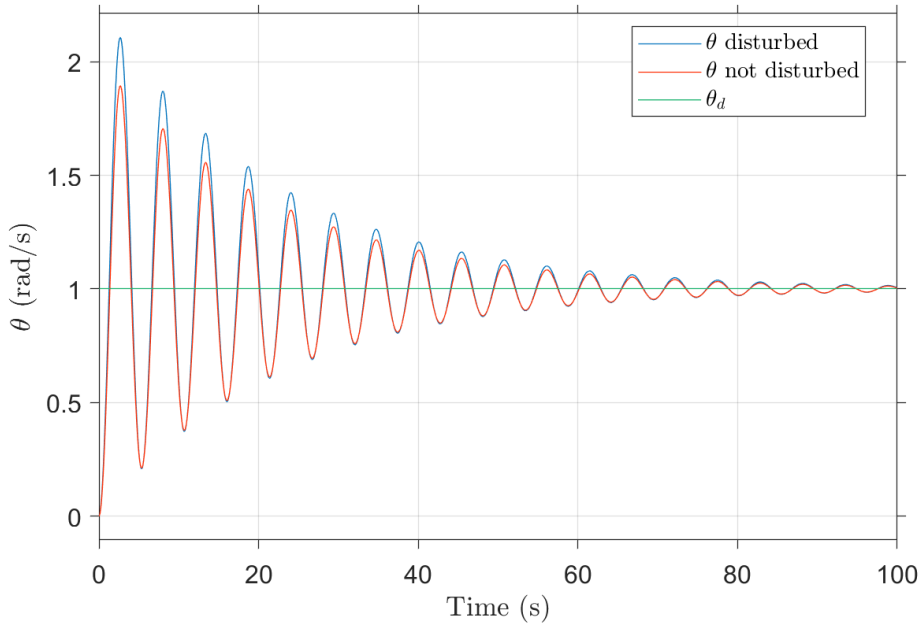

Figure 1.10: Simulation results for θ with and without disturbances for the desired $\theta_d = 1$

1.4 Task 4

In this task, we intend to have a more realistic situation by assuming that the motors are used for a 2-link robot arm.

To incorporate the gravity function into the model, we use the gravity torque vector $G(q)$, which is computed based on the current joint positions of the robot. These torques are added directly as disturbance inputs to each DC motor block, since the motor dynamics are expressed in torque (Nm) and the gravity output matches this unit. By applying the appropriate component of $G(q)$ to each joint, we realistically simulate the effect of gravity on the system without explicitly coupling the joint controllers, in line with the assumptions of independent joint control.

In Fig. 1.11, the complete closed-loop control system implemented in SIMULINK is presented for the 2-link robotic arm, including the gravity function integration. The system includes a PI controller for each motor, properly tuned to minimize overshoot and reduce settling time. A velocity feedback loop is incorporated to introduce damping and improve stability.

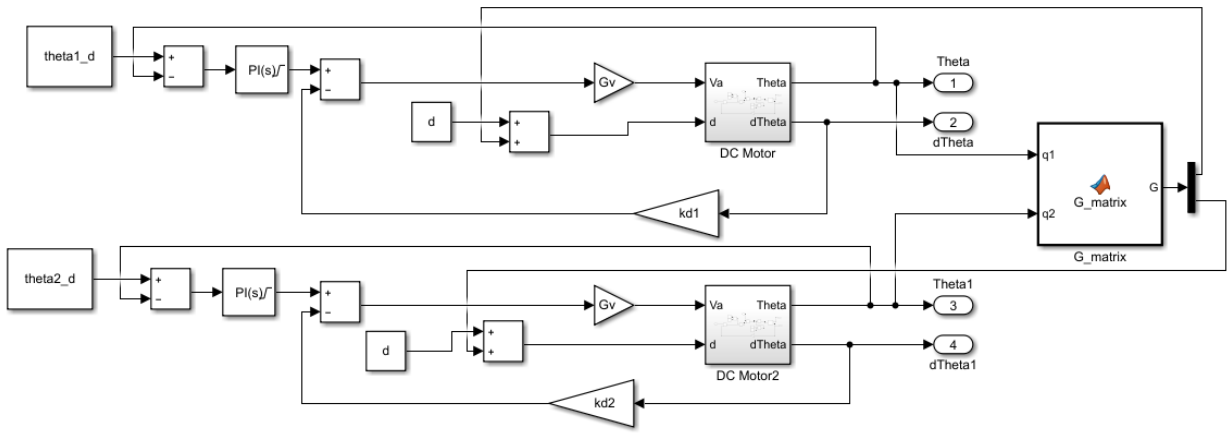

Figure 1.11: Closed-loop control system with PI in the forward path and D implemented via velocity feedback.

The controllers were adjusted to meet the design requirement of an overshoot below 20%, which was successfully achieved. However, due to system limitations and the coupling between joints, the transient response time for joint θ_1 could not be reduced below 15 seconds. The control system parameters used are listed in Table 1.2.

Fig. 1.12 shows the evolution of θ_1 and θ_2 over time, along with the reference set-point $\theta_d = 1$ rad. A dashed horizontal line indicates the 20% overshoot limit at $\theta = 1.2$ rad, and a vertical line marks the 10-second settling time threshold.

Table 1.2: Parameters for each joint controller

Motor	K_p	K_i	K_d
θ_1	64	14	21
θ_2	22.20	8	15

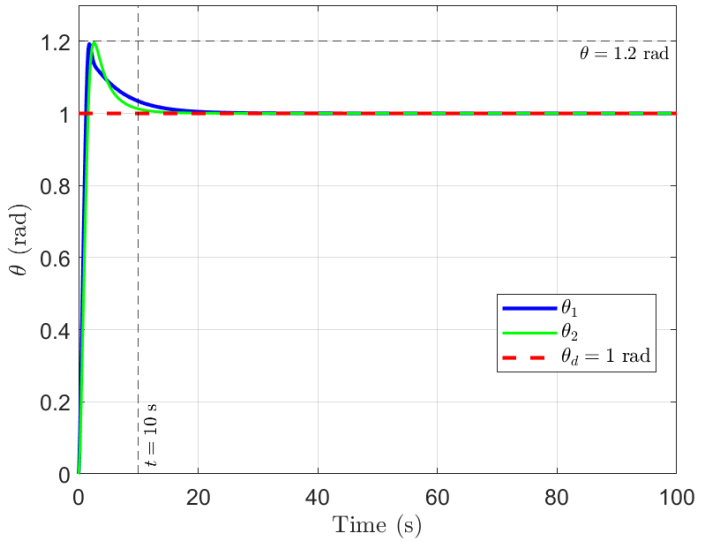

Figure 1.12: Joint position response of the 2-link robot arm for the tuned Controller.

The derivative element D (maked as kd1 and kd2 in Fig. 1.11) , implemented through velocity feedback, helped improve the system's transient response by increasing damping. This reduced overshoot and oscillations, leading to a more stable trajectory toward the desired joint position.